Supporting Information

Corrosion-Resistant Mesoporous Carbon Allowing for Durable, High-Performance Hydrogen Fuel Cells for Heavy-Duty Vehicle Applications

Marwa Atwa[1,+], Sara Pedram[2], Shicheng Xu[1,3], Samuel Dull[4], Yunha Jung[5], Takeharu Yoshii[6], Ruohong Sui[7], Rong Xu[5], Robert Marriott[7], Hirotomo Nishihara[6], Jonathan E. Mueller[8], Marco Wiethop[8], Sebastian Kirsch[8], Gerold Huebner[8], Vedran Glavas[8,9], Jasna Jankovic[2], Thomas Jaramillo[4,10,+], Fritz Prinz[1,3,10,11,+]

1. Department of Mechanical Engineering, Stanford University, Stanford, CA 94305, USA
2. Department of Materials Science and Engineering, University of Connecticut, Storrs, CT 06269
3. Jinetics Inc., 297 Bernardo Ave, Mountain View, CA, 94043, USA
4. Department of Chemical Engineering, Stanford University, Stanford, CA, 94305, USA
5. Department of Materials Science and Engineering, Stanford University, Stanford, CA, 94305, USA
6. Advanced Institute for Materials Research (WPI-AIMR)/Institute of Multidisciplinary Research for Advanced Materials, Tohoku University, Sendai, 980-8577, Japan
7. Department of Chemistry, University of Calgary, 2500 University Dr NW, Calgary, AB, T2N 1N4, Canada
8. Volkswagen AG, Berliner Ring 2, 38440 Wolfsburg, Germany
9. Department of Mechanical Engineering, Mannheim Technical University of Applied, Mannheim, 68163 Germany
10. SUNCAT Center for Interface Science and Catalysis, SLAC National Accelerator Laboratory, Menlo Park, CA 94025, USA
11. Department of Mechanical and Industrial Engineering, Norwegian University of Science and Technology, Trondheim, 7491, Norway

+ Corresponding authors: marwaatw@stanford.edu, jaramillo@stanford.edu, fprinz@stanford.edu

Table S1. Porous structural properties of MCPs, obtained from N_2 gas sorption analysis

Sample	Pore size (nm)[a]	Pore neck size (nm)[b]	BET surface area, S_{BET} (m^2/g)[c]	Microporous surface area, S_{micro} (m^2/g)[d]	S_{micro}/S_{BET} (%)	Pore Volume (ml/g)[e]
MCP8	6.4	4.8	412.5	59.1	14	1.3
MCP12	8.8	4.7	347.2	58.2	17	0.9

[a] The pore diameter in nm, obtained from the adsorption branch, using BJH method.
[b] The pore neck diameter in nm, obtained from the desorption branch, using BJH method.
[c] SBET = total surface area, obtained using the Brunauer−Emmett−Teller (BET) plot in the partial pressure range of $0.05 < P/P0 < 0.30$.
[d] Smicro = total micropore surface area, obtained using the t-plot method in the partial pressure range of $0.2 < P/P0 < 0.5$, with carbon black used as the reference.
[e] Pore volume, determined from N_2 sorption isotherms at $P/P^0 = 0.98$.

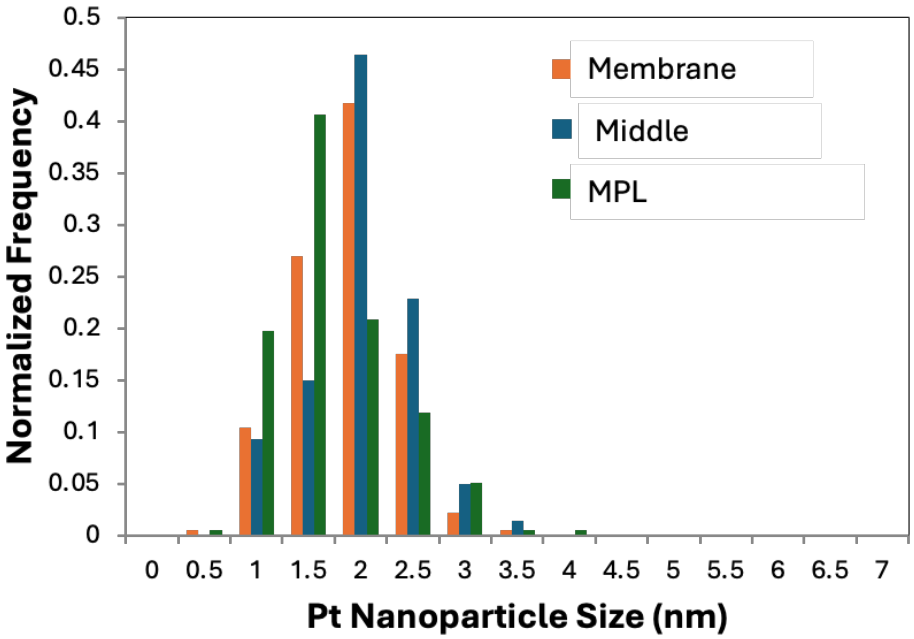

Figure S1. Histogram illustrating the Pt nanoparticle size distribution across distinct regions of the catalyst layer (Pt/MCP8, 0.1 mgPt cm^{-2}), including the central region, membrane-facing side, and MPL-facing side, measured from HR-TEM images.

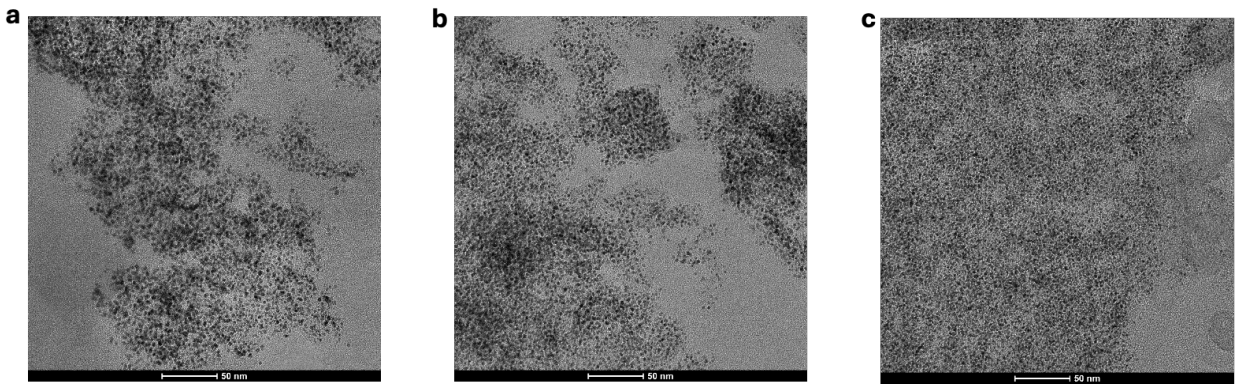

Figure S2. TEM images of Pt/MCP8 with a Pt loading of 0.1 mg Pt/cm² taken at three locations across the catalyst layer: (a) surface facing the membrane, (b) middle of the layer, and (c) interface facing the MPL/GDL.

Table S2. Pt particle size of MCPs-based GDE

Sample	Inner of a carbon	Outer of a carbon
MCP8-BoL	1.44 ± 0.57	1.53 ± 0.63
MCP8-10K	2.58 ± 0.83 (+79%)	4.33 ± 1.79 (+183%)
MCP12-BoL	1.44 ± 0.58	1.53 ± 0.63
MCP12-10K	4.81 ± 0.98 (+234%)	6.50 ± 1.35 (+325%)

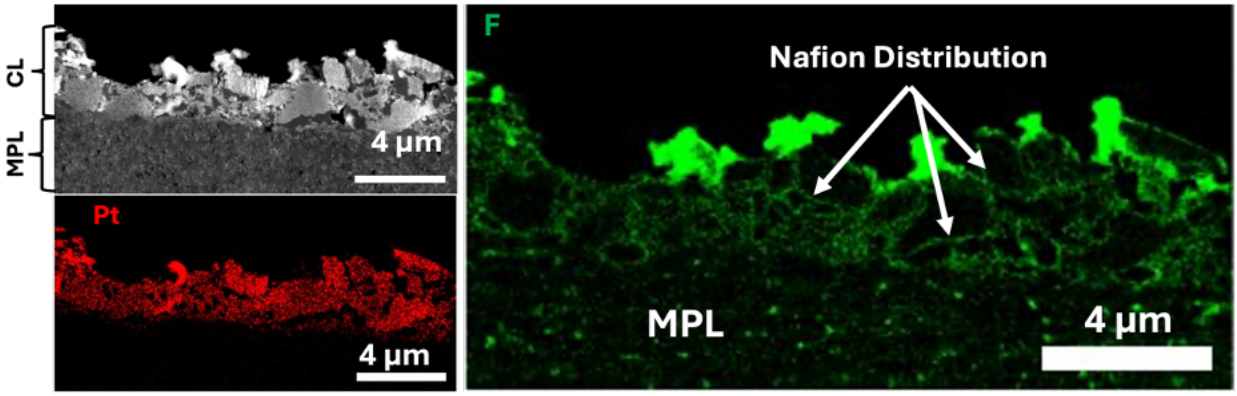

Figure S3. Scanning transmission electron microscope (STEM) image of **Pt/MCP8** GDE cross-section at **BoL,** including energy dispersive X-ray spectroscopy (EDS) analysis of Pt and F.

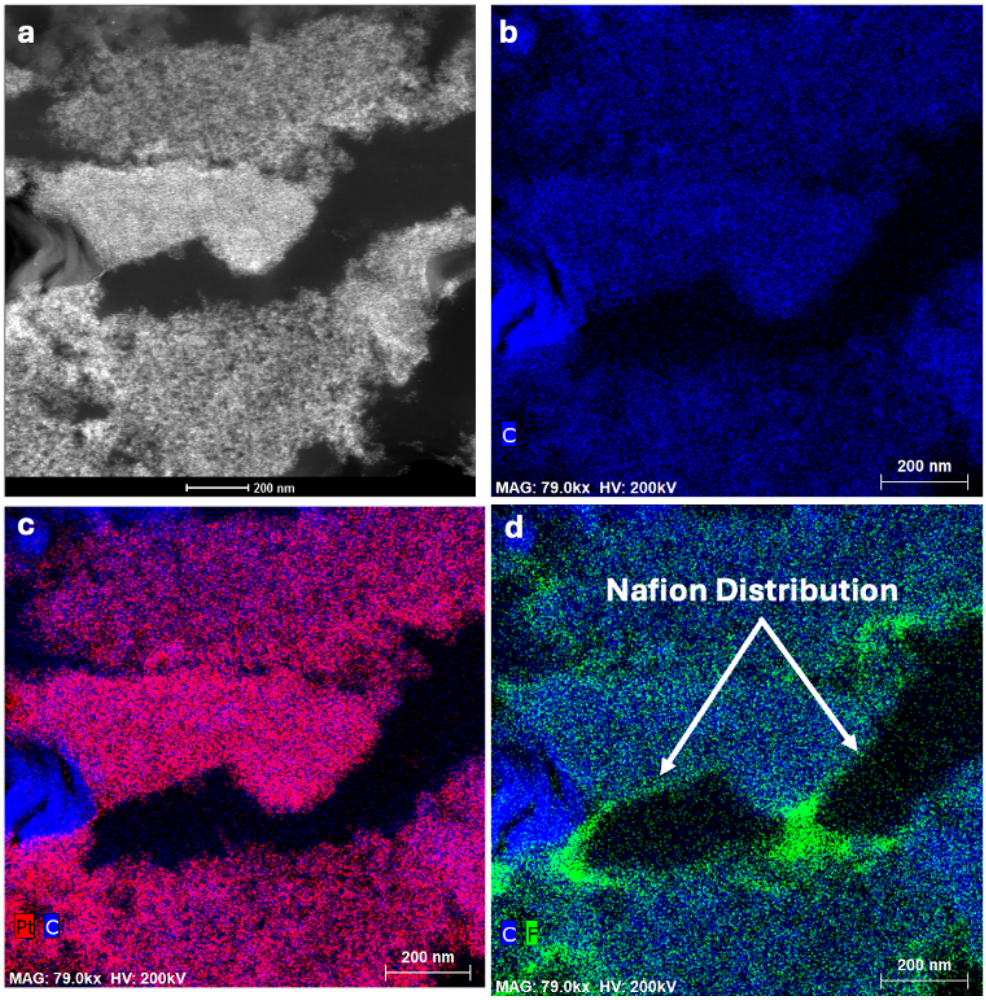

Figure S4. (a) STEM image of **Pt/MCP8** GDE cross-section at **BoL**. (b) Energy dispersive X-ray spectroscopy (EDS) analysis of C. (c) EDS analysis of Pt. (d) EDS analysis of F.

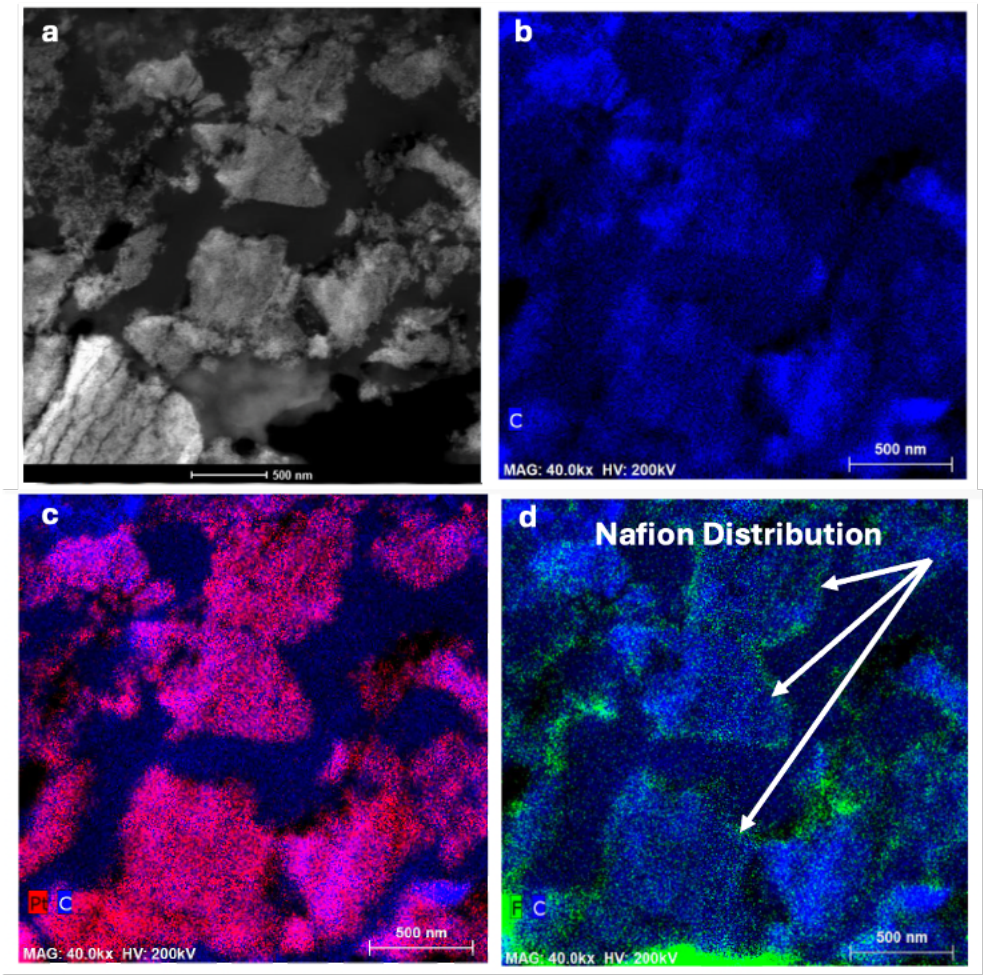

Figure S5. (a) STEM image of **Pt/MCP12** GDE cross-section at **BoL**. (b) EDS analysis of C. (c) EDS analysis of Pt. (d) EDS analysis of F.

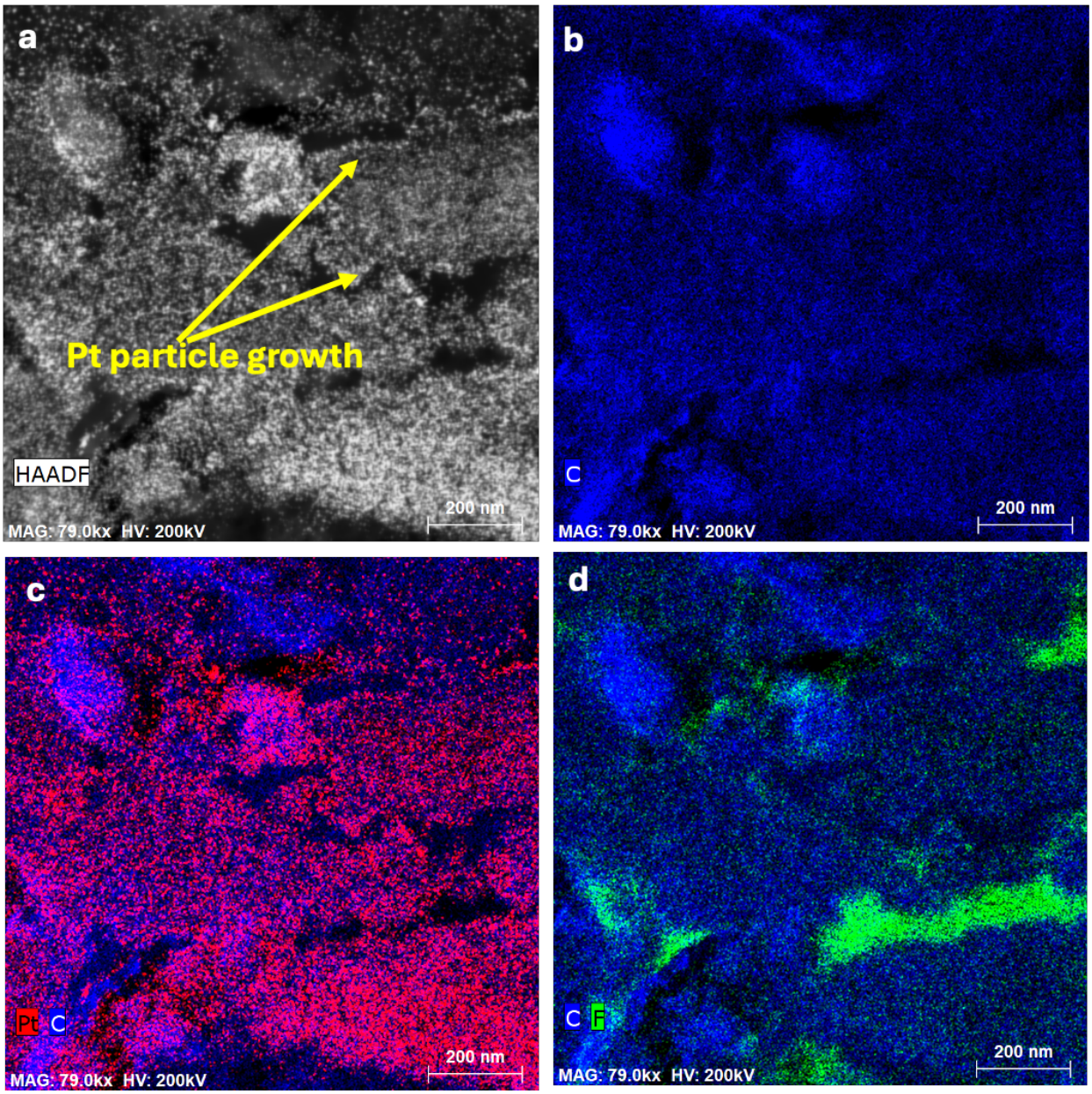

Figure S6. Scanning transmission electron microscope (STEM) image of **Pt/MCP8** GDE cross-section at **EoL (10,000 cycles),** including EDS analysis of Pt and F.

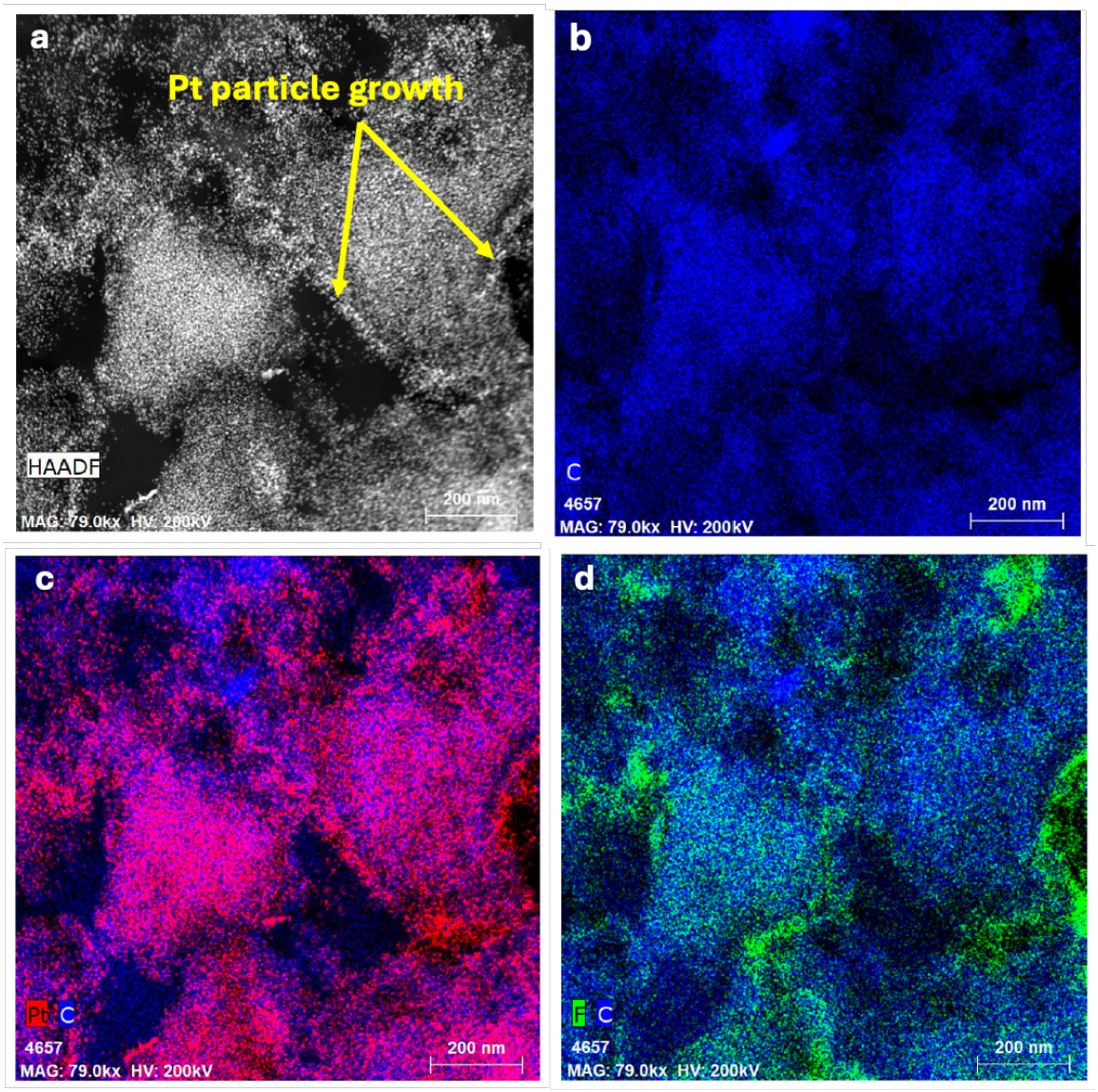

Figure S7. (a) Scanning transmission electron microscope (STEM) image of **Pt/MCP12** GDE cross-section at **EoL (after 10,000 cycles)**. (b) EDS analysis of C. (c) EDS analysis of Pt. (d) EDS analysis of F.

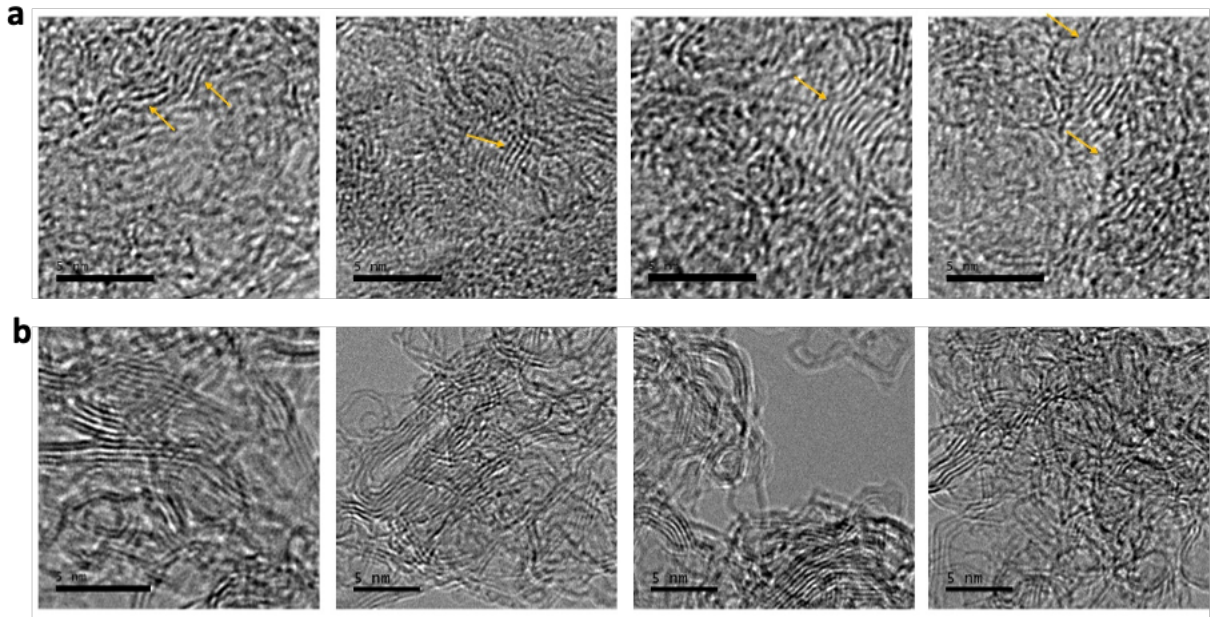

Figure S8. HRTEM images of (a) MCP8 and (b) MCP8-2000 and the presence of multilayer graphene

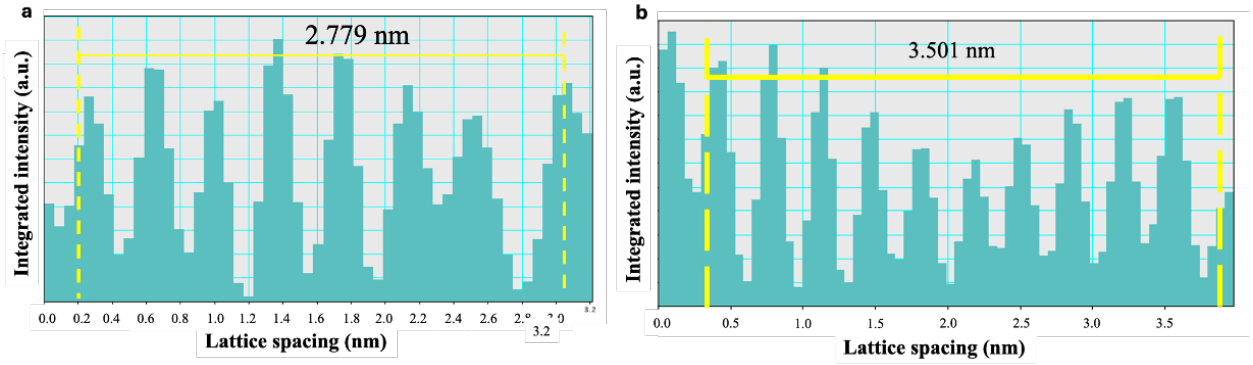

Figure S9. (a) The interplanar spacing measured by integrating a few graphene layers (7 layers) in MCP8 is shown in Figure 5c. (b)The interplanar spacing measured by integrating a few graphene layers (10 layers of MCP8-2000 is shown in Figure 5d.

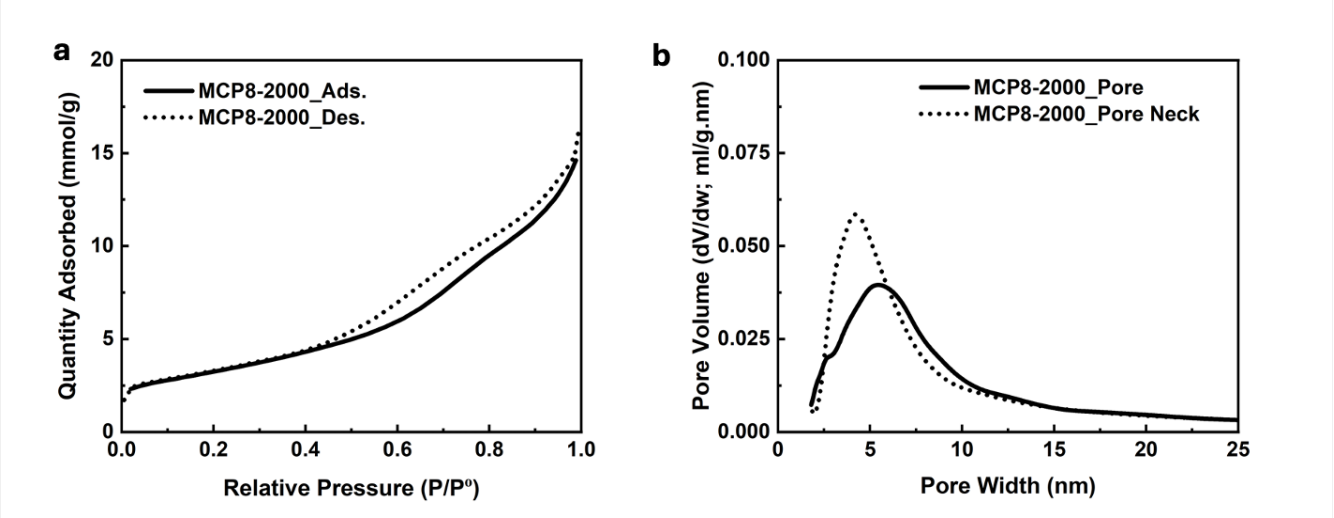

Figure S10. (a) Nitrogen gas sorption analysis of MCP8-2000. (b) Pore size distribution of MCP8-2000 obtained from the N_2 gas sorption isotherm (BJH method), with the adsorption branch (solid lines), giving the average pore diameter, and the desorption branch (dotted lines), giving the average pore neck size.

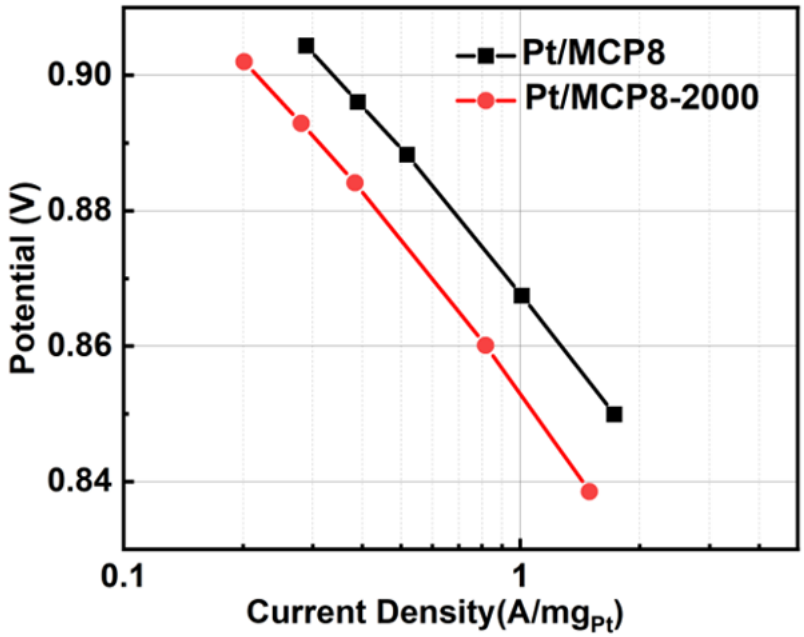

Figure S11. The mass activity of the GDEs of Pt/MCP8 and Pt/MCP-2000 in pure O_2 at 100 % R.H., 150 kPa_{abs}, and 80°C. Pt mass loadings in both GDEs is 0.3 mg_{Pt}/cm^2

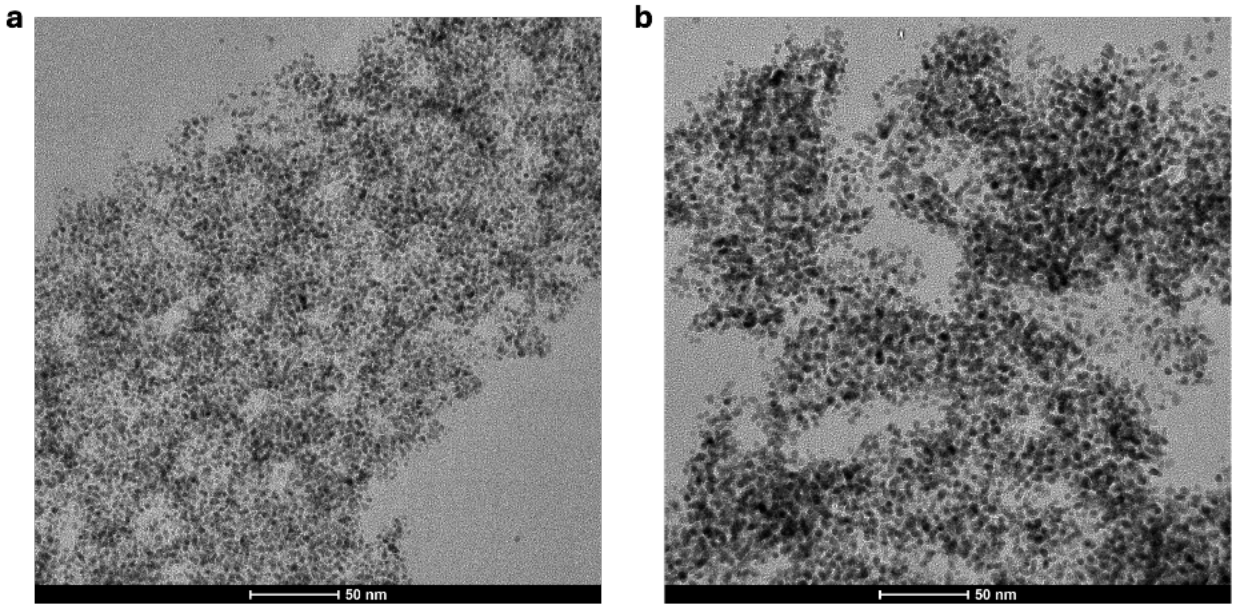

Figure S12. Transmission electron microscope (TEM) images of the GDEs of (a) Pt/MCP8 and (b) Pt/MCP-2000.

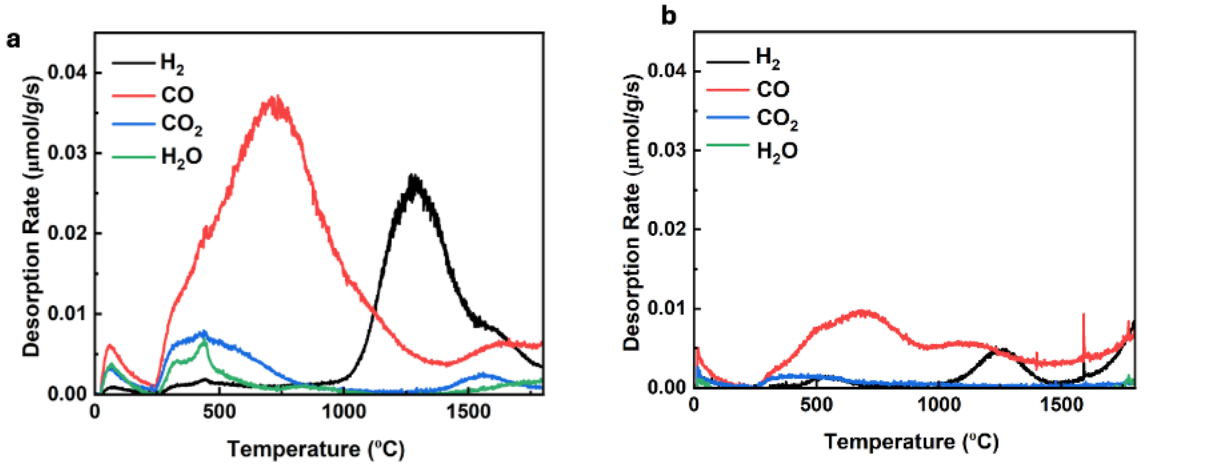

Figure S13. H_2, CO, CO_2, and H_2O production for (a) MCP8 and (b) MCP8-2000 during temperature programmed analysis (TPD) analysis.

Table S3. Amount of gas released from MCPs during TPD analysis.

Sample	H_2 [µmol/g]	H_2O [µmol/g]	CO [µmol/g]	CO_2 [µmol/g]	Total gas evolution [µmol/g] $H_2 + H_2O + CO + CO_2$
MCP8	66	13	143	24	246
MCP8-2000	15	0.4	51	6	72

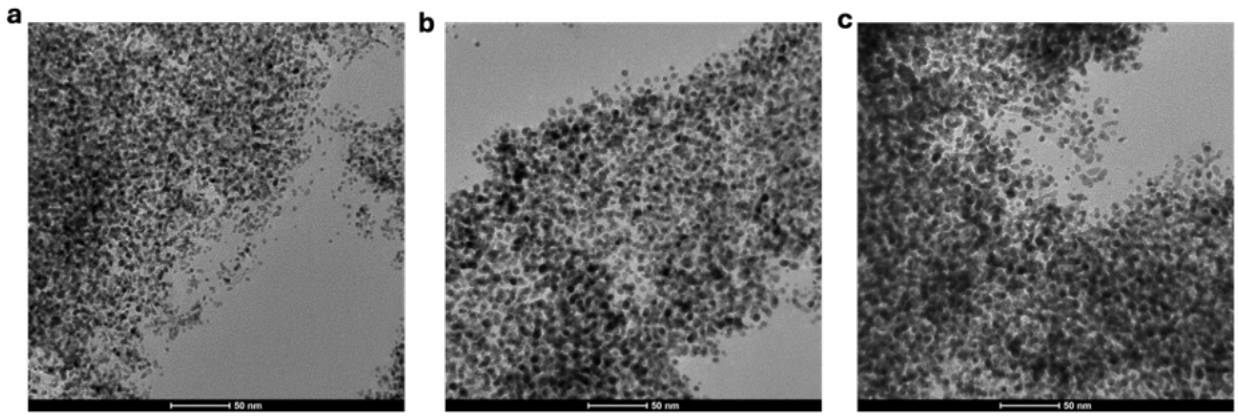

Figure S14. TEM images showing the change in the Pt NPs at (a) BoL (3.25 ± 0.81 nm) and (b) after applying Pt dissolution protocol for 10 k cycles (4.44 ± 1.23 nm) and (c) after applying carbon corrosion protocol (4.26 ± 1.15 nm).

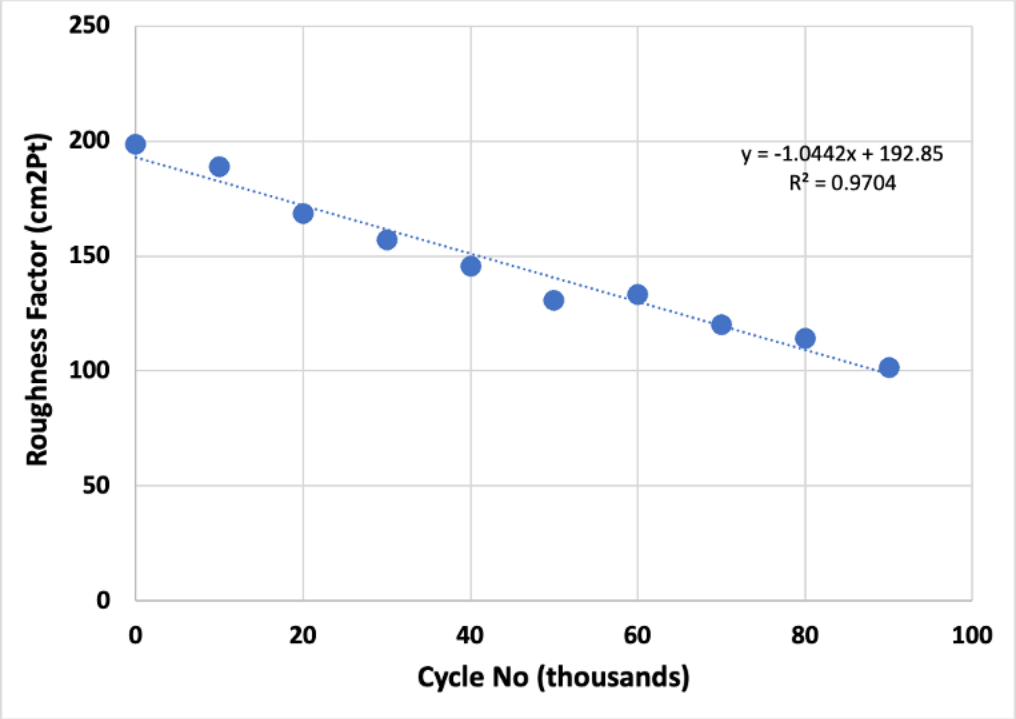

Figure S15. ECSA change of Pt/MCP8-2000 as a factor of Pt dissolution cycles.

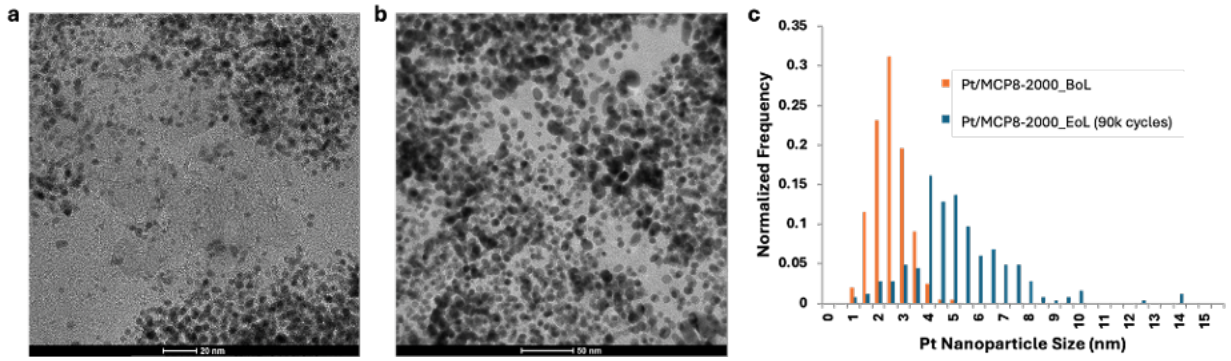

Figure S16. TEM analysis of (a) Pt/MCP8-2000 GDE at the BoL. (b) Pt/MCP8-2000 GDE at the EoL (after 90k cycles). (c) A histogram that shows the distribution of Pt NPs of both (a) and (b)

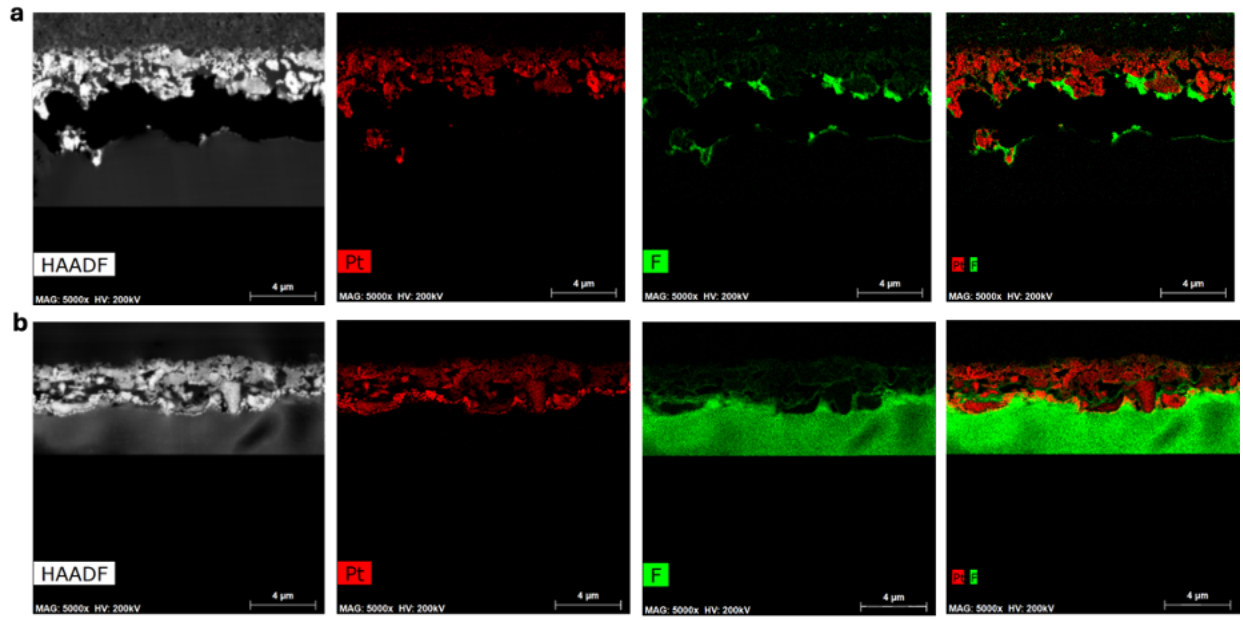

Figure S17. High-Angle Annular Dark-Field (HAADF) - TEM images and EDS maps of Pt and F of microtome cross sections of the (a) Pt/MCP8-2000 (BoL) and Pt/MCP8-2000 MEA (EoL after 90k cycles).

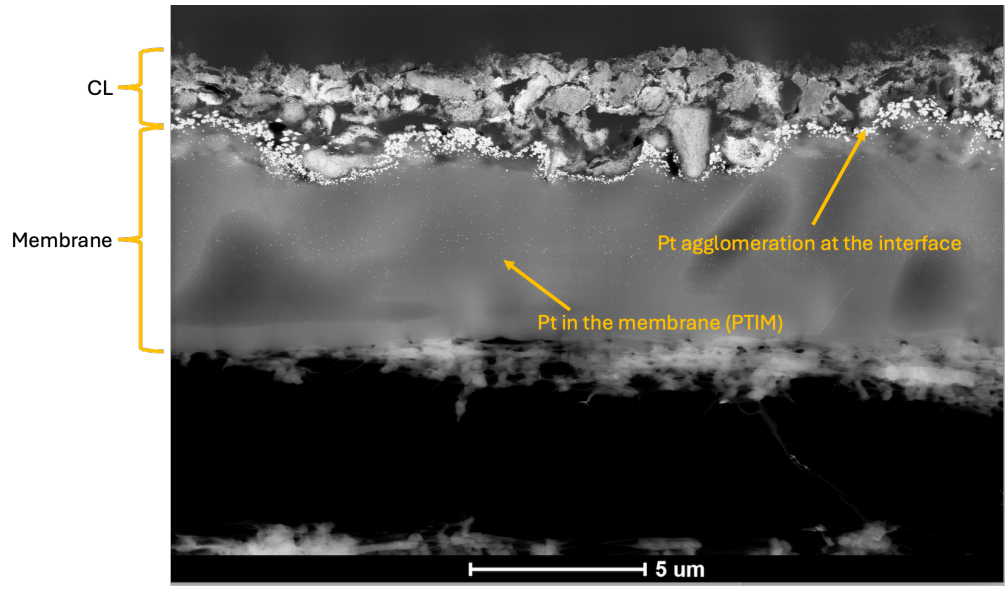

Figure S18. HAADF - TEM images of microtome cross sections of the Pt/MCP8-2000 MEA (EoL after 90k cycles).

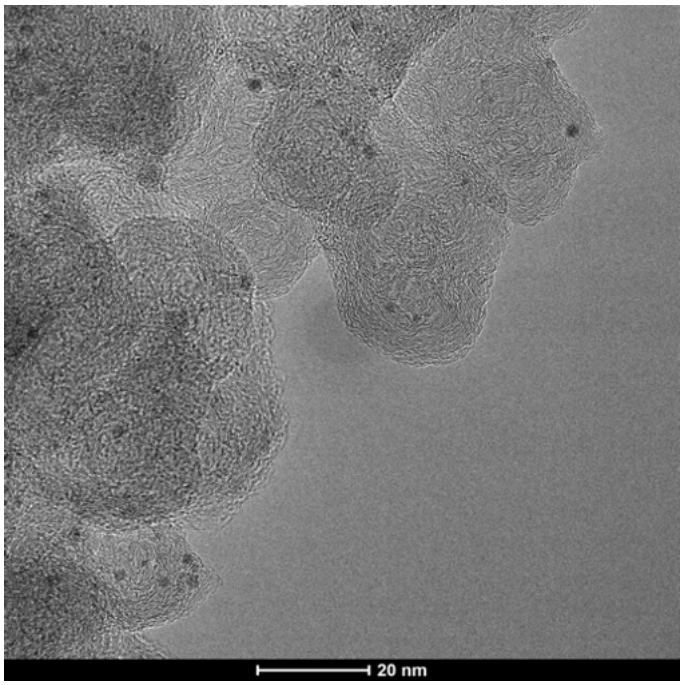

Figure S19. HR-TEM of Pt/MCP8-2000, with the dark contrast indicating Pt NPs deposited on highly graphitic/graphene layer and sheets.